Electric-field-induced magnetization reorientation in a (Ga,Mn)As/(Ga,Mn)(As,P) bilayer with out-of-plane anisotropy

M. Cormier,[1,2] V. Jeudy,[2,3,*] T. Niazi,[1] D. Lucot,[1] M. Granada,[1,†] J. Cibert,[4] and A. Lemaître[1]

[1]*Laboratoire de Photonique et de Nanostructures, CNRS UPR 20, 91460 Marcoussis, France*

[2]*Laboratoire de Physique des Solides, Univ. Paris-Sud, CNRS, UMR 8502, 91405 Orsay Cedex, France*

[3]*Université de Cergy-Pontoise, 95000 Cergy-Pontoise, France*

[4]*Institut Néel, CNRS, Univ. Joseph Fourier, UPR 2940, 38042 Grenoble, France*

(Received 11 July 2014; revised manuscript received 29 September 2014; published 14 November 2014)

Combined electric- and magnetic-field control of magnetization orientation and reversal is studied using anomalous Hall effect in an ultrathin ferromagnetic (Ga,Mn)As/(Ga,Mn)(As,P) bilayer. Its anisotropy results from the electrically tunable competition between the in-plane and out-of-plane anisotropies of both layers. The magnetic hysteresis loop shape is sensitive to the bias electric field. In the loop reversible part, an electric-field variation is found to reorient reversibly the magnetization. In this case, the magnetization direction follows the easy anisotropy direction controlled by electric field. In contrast, in the hysteretic part, an almost complete nonreversible magnetization reversal is achieved. This is interpreted as resulting from the electric-field-induced enhancement of domain nucleation and domain-wall propagation.

DOI: 10.1103/PhysRevB.90.174418 PACS number(s): 75.60.Ej, 75.30.Gw, 75.50.Dd, 75.50.Pp

I. INTRODUCTION

Controlling magnetism in thin-film structures without magnetic field has recently motivated an intense research effort. In particular, the control of the magnetization with an electric voltage has been demonstrated in a variety of systems [1–5]. These demonstrations have opened the road to new spintronic devices, exhibiting ultralow electrical consumption. Moreover, new manipulation schemes relying on electric field have been proposed such as switching using electrical pulses [6–10] or electric-field-assisted domain-wall motion [11–13]. To test these new concepts, the archetypal diluted magnetic semiconductors (Ga,Mn)As and (In,Mn)As have been an interesting playground. Indeed, in these materials, the ferromagnetic properties are largely controlled by the carrier density. In ultrathin single magnetic layers embedded in field-effect devices, where sizable carrier depletion can be achieved by electric field, the Curie temperature and the magnetic anisotropy could be controlled [1,3,13–16]. However, these devices suffer from several limitations. First, to achieve large carrier depletions, the carrier density has to be set close to the metal-insulator transition. This leads to complex magnetic configurations, with coexisting ferromagnetic and paramagnetic phases [16]. Even in this situation, the anisotropy changes upon applying an electric field have been rather limited, leading the magnetic easy axis to rotate by few degrees only [3]. Second, these rotations have been investigated for layers with strong in-plane anisotropy. In that case, the magnetization control remains limited to the plane directions. Obviously, extending the electric control of the magnetization to any arbitrary direction would be highly desirable.

Recently, we have demonstrated that in a (Ga,Mn)As/(Ga,Mn)(As,P) bilayer with two competing in-plane and out-of-plane magnetic-anisotropy components, a rather large modulation of the resulting in-plane bilayer anisotropy could be obtained upon applying an electric field, for a relatively moderate depletion, and quite far from the Curie temperature [17]. In this paper, we have further extended this concept to a similar bilayer exhibiting a perpendicular anisotropy under zero electric field. We show electric field control of the magnetic easy axis alignment either along or perpendicular to the growth axis. Two different magnetization manipulation regimes are evidenced. The first one is a coherent rotation of the magnetization over several tens of degrees, observed at sufficiently high magnetic field. The rotation angle is driven by the anisotropy-field dependence on electric field. At low magnetic field, a second regime is observed, characterized by an incoherent magnetization reversal. In that case, reversal occurs in a nonreversible way by nucleation, propagation, and reorganization of magnetic domains.

II. SAMPLE STRUCTURE AND EXPERIMENTAL METHODS

This study is based on an ultrathin (Ga,Mn)As/(Ga,Mn)(As,P) bilayer grown on a (001) GaAs/AlAs buffer [Fig. 1(a)], analogous to the one described in our previous work [17]. In this structure, two competing anisotropies are present: [001] is an easy axis of magnetization in (Ga,Mn)(As,P), while it is a hard axis in (Ga,Mn)As [18]. The bilayer magnetization can be considered as homogeneous along the growth direction since the exchange length is larger than the bilayer thickness. Hence, the effective bilayer magnetic anisotropy results from the balance between these two sources of anisotropy [17]. This balance is controlled by the carrier distribution among the two layers since the ferromagnetism is carrier mediated. In a metal/oxide/(Ga,Mn)As field-effect device, the carrier distribution is mostly affected by the electric field in the upper layer close to the semiconductor-oxide interface [19], here the (Ga,Mn)As layer [Fig. 1(a)]. Hence, applying a positive (resp.

*vincent.jeudy@u-psud.fr

†Present address: Centro Atómico Bariloche, Comisión Nacional de Energía Atómica, Bariloche, Río Negro, Argentina.

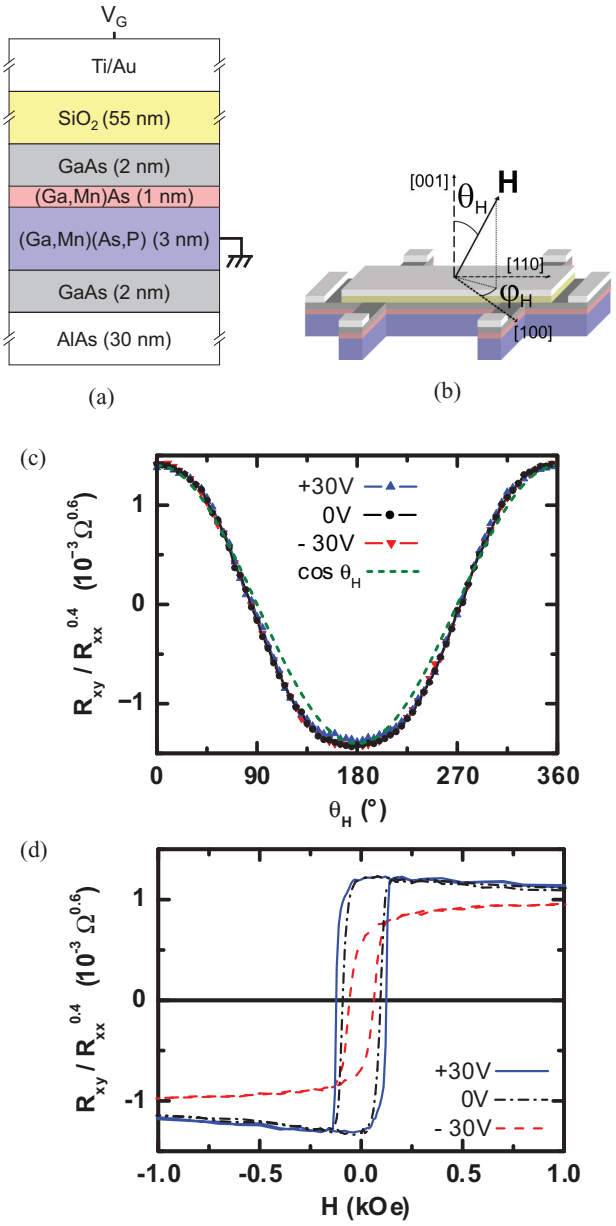

FIG. 1. (Color online) (a) Schematic diagram of the stack structure, showing the magnetic bilayer embedded in a field-effect device. (b) Hall bar schematic drawing indicating the crystallographic directions and magnetic-field orientation. The magnetization orientation is described by θ and φ angles within the same coordinate system (not shown for clarity reasons). (c) Dependence of the Hall resistance on the magnetic-field orientation for $V_G = 0, \pm 30$ V, respectively, measured at 15 K under a constant 6 kOe saturating magnetic field, applied at θ_H from [001], in the (010) plane ($\varphi_H = 45°$). A scaled $\cos\theta_H$ curve (dashed line) is plotted for comparison. (d) Magnetic-field dependence of the Hall resistance, measured at 15 K for $V_G = 0, \pm 30$ V, respectively. The magnetic field was applied at $\theta_H = 50°$ from [001], in the (010) plane ($\varphi_H = 45°$).

negative) gate voltage to the bilayer structure strengthens (resp. weakens) the perpendicular anisotropy.

The GaAs/AlAs buffer was grown at ~550 °C. Then, the rest of the stack, including the bilayer, was grown at a lower ~220 °C temperature. A 105-min post-growth annealing at 200 °C was performed, so as to remove interstitial Mn ions. The effective Mn moment concentration after annealing is about 5%, as known from calibration measurements on thicker samples [20]. Hall bars [215 μm long, 40 μm wide, see Fig. 1(b)] were processed along the [110] direction, using optical lithography and chemical etching, and contacted with Ti (20 nm)/Au (200 nm) pads. An insulating SiO_2 (55 nm) layer was then deposited by plasma-enhanced chemical vapor deposition at 200 °C. Finally, Ti/Au gate electrodes were deposited over the conductive channels, to complete the field-effect architecture.

The longitudinal and transverse resistivities of the Hall bars, ρ_{xx} and ρ_{xy}, respectively, were measured keeping the current low (1 μA), so that the voltage drop across the Hall bar was negligible as compared to the gate voltage V_G. The gate-voltage excursion was limited by the breakdown voltage to ± 30 V (corresponding to an electric field of ± 5.5 MV cm^{-1}). At 4 K, the sheet hole concentration was estimated to $p = 8.3 \times 10^{13}$ cm^{-2} and the ± 30 V gate-voltage excursion yields a change of sheet density of $\Delta p \sim 2.4 \times 10^{13}$ cm^{-2}. We used the constant mobility model of Ref. [3], using a SiO_2 dielectric constant of 3.9. $\Delta p/p$ is moderate compared to previous reports [3]. This is due to the low SiO_2 dielectric constant and to a rather large carrier density. The Curie temperature T_C was derived from the temperature dependence of the bilayer sheet resistance. It is around 60 K for $V_G = 0$ V. Its variation is about 3 K between $V_G = \pm 30$ V, consistent with the rather moderate change of carrier density with gate voltage.

The magnetic properties of our system were investigated through the measurement of the bilayer magnetization out-of-plane component $M_\perp = M \cos\theta$ [Fig. 1(b)]. For this purpose, we relied on the anomalous Hall effect (AHE) [21,22]. Phenomenologically, the transverse resistivity of a magnetic layer is usually written as $\rho_{xy} \approx R_{\rm AHE} M_\perp$, where $R_{\rm AHE}$ is the anomalous Hall effect coefficient. $R_{\rm AHE}$ is known to scale with ρ_{xx}, which depends on both the magnetic field (through a small magnetoresistance of about 4% over the investigated magnetic-field range), and the electric field (through changes in the carrier density). The small planar Hall effect contribution is not taken into account. Given the low conductivity ($\sigma_{xx} \approx 100$ S cm^{-1} and $\sigma_{xy} \approx 3$ S cm^{-1} at 15 K and at magnetic saturation for $V_G = 0$ V), the so-called "dirty" AHE regime is likely to apply to our system, corresponding to a damped intrinsic Berry-phase mechanism, as described in a recent unified AHE theory [23,24]. This gives rise to a $\rho_{xy} \propto \rho_{xx}^{0.4}$ scaling law,[1] in agreement with various experimental results on (Ga,Mn)As layers within this conductivity range [23,25]. Therefore, the variations of $\rho_{xy}/\rho_{xx}^{0.4}$, or $R_{xy}/R_{xx}^{0.4}$ in terms of resistances, under magnetic or electric field should directly reflect variations of $M_\perp$.

The validity of this scaling law was experimentally verified by measuring the $R_{xy}(\theta_H)/R_{xx}^{0.4}(\theta_H)$ ratio as a function of the orientation of a strong rotating magnetic field ($H = 6$ kOe). Here, θ_H is the magnetic-field angle with the film normal. The applied field, much larger than the anisotropy fields, as it will be shown later, is sufficient to align the magnetization along the magnetic-field direction ($\theta = \theta_H$). In that case,

[1]This is equivalent to a $\sigma_{xy} \propto \sigma_{xx}^{1.6}$ scaling.

$M_\perp = M_s \cos\theta_H$, where M_s is the magnetization at saturation. As we can see in Fig. 1(c), the variations of $R_{xy}/R_{xx}^{0.4}$ as a function of θ_H for a given V_G nearly follow the expected $\cos\theta_H$ law. This confirms that $R_{xy}/R_{xx}^{0.4}$ is a good indicator of $M_\perp$. The small differences observed with a pure cosine law are due to higher-order terms in $\cos\theta$, attributed to Berry-phase effects [26]. Besides, the curves obtained for $V_G = 0, \pm 30$ V, respectively, perfectly overlap with each other in Fig. 1(c), which indicates M_s varies only little with electric field. This is consistent with the fact that the measurements were taken at low temperature (15 K), far below T_C where the magnetization at saturation remains constant [3]. In the following, we therefore assume that the changes of $R_{xy}/R_{xx}^{0.4}$ with magnetic or electric field directly reflect the changes of the angle θ between the magnetization vector and the film normal.

III. ELECTRIC-FIELD CONTROL OF THE MAGNETIC ANISOTROPY

A. Gate-voltage modification of the anisotropy

For a better sensitivity to the out-of-plane, in-plane, or canted magnetization orientation, the typical magnetic hysteresis loops presented in Fig. 1(d) were measured under a canted magnetic field applied in the (010) plane ($\varphi_H = 45°$), at $\theta_H = 50°$ from [001] [see Fig. 1(b)]. They correspond to $V_G = 0, \pm 30$ V, respectively, at 15 K. For $H = \pm 6$ kOe, the saturation levels of the loops differ by less than 2% for $V_G = 0, \pm 30$ V, which is consistent with a negligible variation of M_s with electric field. However, for moderate applied magnetic fields, the loops have very different shapes depending on V_G. For $V_G = 0$ and $+30$ V, the out-of-plane magnetization component increases when $|H|$ decreases, which indicates a dominant out-of-plane ($\theta < 50°$) magnetic anisotropy. On the contrary, for $V_G = -30$ V, $M_\perp$ decreases, which indicates a dominant in-plane ($\theta > 50°$) anisotropy. This shows that a large electric-field-induced spin reorientation is achieved [27,28], from a dominant out-of-plane anisotropy ($V_G \geqslant 0$) to a dominant in-plane anisotropy ($V_G = -30$ V). Consistently with our previous results on a similar bilayer (though with slightly different anisotropy properties) [17], a positive (negative) V_G reinforces (weakens) the bilayer out-of-plane anisotropy. In the present sample, the out-of-plane anisotropy contribution associated with the (Ga,Mn)(As,P) layer dominates for $V_G \geqslant 0$ V, probably due to a slightly different interface state with SiO_2, as compared to our previous study [17]. A rough estimate of the reorientation angle can be obtained from a comparison of the hysteresis-loops remanence levels, assuming that the easy axis is not far from out of plane for $V_G = +30$ V. Within this assumption, the reorientation angle between $+30$ and -30 V is $\Delta\theta \approx 60°$, much larger than for previous studies. As we shall understand now, this property is related to our specific anisotropy configuration, a weak anisotropy in zero electric field, and a rather large sensitivity of our device anisotropy to the electric field.

B. Reorientation of the easy magnetization direction

In order to get a quantitative understanding of the observed electric-field-induced magnetization reorientation, the bilayer magnetic anisotropy was calculated starting from a free-energy model. For (Ga,Mn)As, the free energy can be parametrized as follows [29]:

$$F = \frac{M}{2}\Big\{ -2H[\cos\theta\cos\theta_H + \sin\theta\sin\theta_H\cos(\varphi-\varphi_H)] + H_{2\perp\text{eff}}\cos^2\theta - \frac{H_{4\perp}}{2}\cos^4\theta - \frac{H_{4\parallel}}{8}(3+\cos 4\varphi)\sin^4\theta - H_{2\parallel}\sin^2\left(\varphi-\frac{\pi}{4}\right)\sin^2\theta\Big\}, \quad (1)$$

where $H_{4\perp}$ is the perpendicular cubic anisotropy field, and $H_{2\parallel}$ and $H_{4\parallel}$ are the in-plane uniaxial and cubic anisotropy fields, respectively. $H_{2\perp\text{eff}}$ is defined by $H_{2\perp\text{eff}} = 4\pi M_s - H_{2\perp}$, where $H_{2\perp}$ is the perpendicular uniaxial anisotropy field. The angles θ, φ, θ_H, and φ_H are defined in Fig. 1(b).

The anisotropy fields were determined, at 4 K, from Hall resistance measurements, following a procedure described by others [21,22] and used in Ref. [17], for several V_G values. The applied magnetic field was rotated from $\theta_H = 0$ to 2π, successively in the $\varphi_H = 0$, $\frac{\pi}{4}$, and $\frac{\pi}{2}$ planes. The applied magnetic field ($H = 500$ Oe) was set larger than the coercive field, so as to ensure a coherent magnetization rotation. For each φ_H value, a function minimizing the free energy (i.e., verifying $\partial F/\partial\theta = 0$) was fitted to the θ_H dependence of the Hall resistance, and the anisotropy fields were deduced as fitting parameters. The above-mentioned higher-order terms in $\cos\theta$ were taken into account. While doing this, the magnetization direction was assumed to remain always in the magnetic-field rotation plane, that is, $\varphi = \varphi_H$. For $\varphi_H = 0$, $\frac{\pi}{4}$, and $\frac{\pi}{2}$, this hypothesis is compatible with $\partial F/\partial\varphi = 0$, provided that $|H_{2\parallel}|$ is small as compared to $|H|$ and to the other anisotropy fields.

The anisotropy-fields variations with V_G, obtained within this assumption, are reported in Fig. 2. They exhibit a smooth evolution with electric field except for $H_{4\perp}$ whose values appear more scattered. These experimental fluctuations

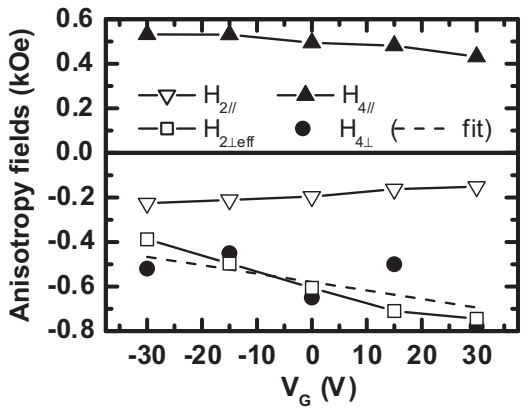

FIG. 2. Experimental values of the four anisotropy fields of the magnetic bilayer, as functions of the gate voltage V_G. Measurements were performed at 4 K, under a rotating 500 Oe magnetic field. $H_{2\perp\text{eff}}$ is defined as $4\pi M_s - H_{2\perp}$. The dashed line is a linear fit to $H_{4\perp}$ data points.

arise from the difficulty to extract the contributions of each anisotropy field, when these fields are weak and of the same order of magnitude. In the following, we use a linear fit for $H_{4\perp}$ (dashed line) to filter out these fluctuations. For technical reasons, the anisotropy measurements could only be performed at 4 K instead of 15 K for the magnetization reorientation measurements. This can lead to a slight overestimation of the anisotropy fields at 15 K [20]. An additional source of error originates from the non-negligible value of $H_{2\parallel}$, compared to the other anisotropy and applied fields, in particular for V_G close to -30 V. However, as we shall see now, these anisotropy fields are compatible with the magnetization reorientation measurements presented in the following. $H_{2\parallel}$ and $H_{4\parallel}$ hardly vary with electric field, while $H_{2\perp\text{eff}}$ and $H_{4\perp}$ change over several hundreds of oersted. This behavior is expected, as the effective device anisotropy results from a balance between the two-layer opposite anisotropies.

The easy magnetization direction can be deduced from Eq. (1) with the anisotropy-field values determined experimentally. In layers with a strongly dominant uniaxial anisotropy, the easy axis direction, in plane or out of plane, is given by the sign of $H_{2\perp\text{eff}}$. Here, as all the anisotropy fields are comparable, the easy axis direction is given by a complex interplay between the different anisotropy fields. It is necessary therefore to resort to numerical calculations to find the magnetization angles corresponding to free-energy minima. Selected free-energy landscapes are reported in Figs. 3(a)–3(f). As it can be observed, for $H = 0$ Oe [Figs. 3(a)–3(c)], the easy axis is aligned along the [001] direction (out-of-plane anisotropy) for $V_G \geqslant 0$ V, while for $V_G = -30$ V, the free energy has two equivalent minima corresponding to two easy axes in the film plane. This confirms the strong sensitivity of the bilayer easy axis to the electric field, especially for $V_G < 0$, in good agreement with the results from Fig. 1(d). However, the in-plane easy axes predicted from these anisotropy-field values at $V_G = -30$ V appear to be in contradiction with the nonzero remanent perpendicular component of the magnetization observed in Fig. 1(d) at the same gate voltage. This results from the very weak perpendicular anisotropy at $V_G = -30$ V. The free-energy simulation indicates that a perpendicular magnetic field of a few oersted is sufficient to reorient the magnetization along the growth axis, and to bring $\cos\theta$ back to a finite value. We therefore attribute this nonzero remanent component to anisotropy inhomogeneities. The accuracy of the simulated perpendicular component can be compared to direct measurements, as shown in Fig. 3(g). Here, $M_\perp/M_s = \cos\theta$ is plotted as a function of V_G. A rather good agreement is obtained for various magnetic field strengths and orientations. A systematical magnetization reorientation toward the plane is observed as V_G decreases. Namely, for $H = 200$ Oe, $\theta_H = 50°$, and $\varphi_H = 45°$, the easy axis is oriented about $\theta = 29°$ from the [001] direction at $V_G = +30$ V, and it is tilted down to $\theta = 53°$ at $V_G = -30$ V, consistent with the easy axis orientations obtained from Figs. 3(d)–3(f). The value measured at $H = 0$ Oe and $V_G = -30$ V is compared to the simulation obtained for a small (∼5 Oe) magnetic field applied along the growth axis. The good agreement indicates the strong sensitivity of the magnetization to anisotropy inhomogeneities, as discussed above.

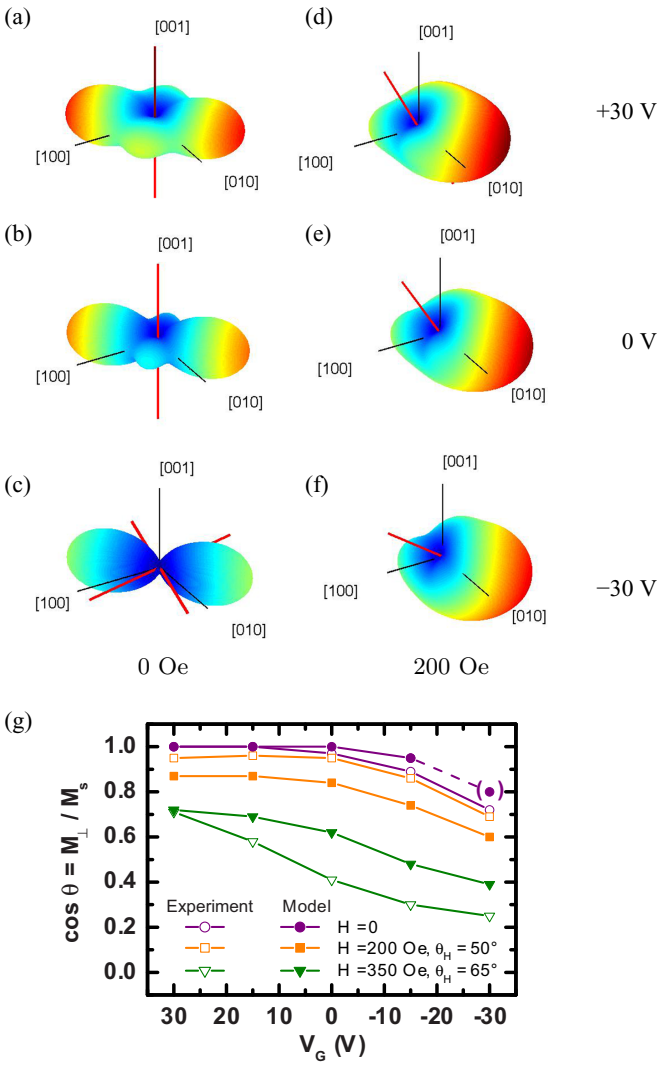

FIG. 3. (Color online) (a)–(f) Three-dimensional free-energy landscapes in polar coordinates, for $V_G = +30$ V [(a),(d)], 0 V [(b),(e)], and -30 V [(c),(f)], under an applied magnetic field $H = 0$ [(a)–(c)], and $H = 200$ Oe [(d)–(f)]. Magnetic-field points at $\theta_H = 50°$ and is applied in the (010) plane ($\varphi_H = 45°$). The color scale indicates the relative magnitude of the calculated free energy. Easy axes corresponding to the global free-energy minima are indicated by red lines. (g) Comparison between predicted and measured out-of-plane projections of the magnetization, for different applied-magnetic-field values. Measurements were performed in a magnetic state which reversibly responds to the applied electric field. For the point in parentheses, a small (∼5 Oe) magnetic field applied along the growth axis was assumed in the simulation.

IV. ELECTRIC-FIELD SWITCHING OF THE MAGNETIZATION

A. Combined electric- and magnetic-field effects

The evolution of the sample magnetic state, under a combined magnetic- and electric-field cycling, was investigated following the experimental protocol described in Fig. 4(a). Initially, V_G was fixed to $+30$ V, and the magnetization was saturated with $H = -6$ kOe. H was then increased (1), and stopped (2) at a pause field H_p. Next, a gate-voltage cycling

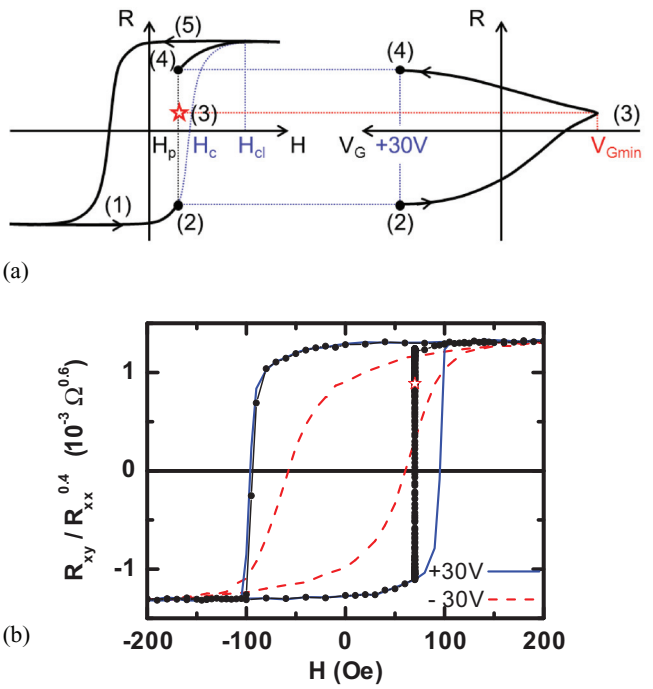

FIG. 4. (Color online) (a) Schematic description of the combined magnetic- and electric-field-cycling experiments. The coercive field H_c, the pause field H_p, and the closure field H_{cl}, beyond which the system is magnetically monodomain, are defined. The star indicates the point reached when the gate voltage reaches its minimum value V_{Gmin}. (b) Magnetic-field dependence of the Hall resistance at 15 K, with the magnetic field applied along [001]. The solid- and dashed-line loops (reference loops) were measured under a constant gate voltage ($V_G = \pm 30$ V, respectively). For the other loop (symbols), the initial gate voltage was +30 V. After saturation under $H = -6$ kOe, the magnetic field was fixed at $H_p = 70$ Oe, and the gate voltage was varied (≈ 1 V s^{-1}) from +30 to −30 V, where the point indicated by a star was reached. Then, V_G was increased back to +30 V, before the rest of the magnetic hysteresis loop was measured.

was performed under $H = H_p$: V_G was decreased down to V_{Gmin} (3), and then increased back and fixed again to +30 V (4). Finally, H was varied under $V_G = +30$ V, so as to describe the rest of the magnetic hysteresis loop (5). The magnetic relaxation at 15 K was found to be negligible for $V_G = +30$ V at each H_p, so that modifications of the magnetic state between (2) and (4) essentially reflect the effects of electric-field cycling.

A first example of such effects is depicted in Fig. 4(b), where reference magnetic hysteresis loops, measured under a constant $V_G = \pm 30$ V, respectively, are also reported for comparison. For this experiment, H was applied along the out-of-plane easy axis of magnetization [see Fig. 3(a)]. Upon varying V_G, a strong, nonreversible variation of the Hall resistance is clearly visible [states (2) and (4) of Fig. 4(a) are different]. Namely, the electric cycle between +30 and −30 V under $H_p = 70$ Oe (that is only 74% of the coercive field for $V_G = +30$ V) results in a nearly complete transition between the two metastable states corresponding to opposite out-of-plane magnetizations.

To get a further insight into the effects of a combined magnetic and electric cycling, a more systematic study was performed under a canted magnetic field. With such a geometry, magnetic-hysteresis-loop changes with V_G are indeed much more visible than under an out-of-plane magnetic field, as it can be seen in Fig. 1(d). Typical loops obtained for $\varphi_H = 45°$, $\theta_H = 50°$, and $V_{Gmin} = -30$ V are reported in Fig. 5(a), together with reference magnetic hysteresis loops recorded for constant $V_G = \pm 30$ V, respectively. The corresponding variation of $M_\perp$ with V_G during the electric cycles [between states (2) and (4) in Fig. 4(a)] is shown in Fig. 5(b). Starting from a magnetic monodomain, that is, for a H_p value (=200 Oe) larger than the closure fields of both reference loops [$H_{cl}(+30$ V) and $H_{cl}(-30$ V), beyond which the magnetization varies reversibly, even if saturation is not yet reached, see Fig. 4(a)], the electric-field cycle produces a reversible variation of $M_\perp$, as it can be observed in Fig. 5(b). In contrast, for an H_p value (=30, 50, and 100 Oe) lower than $H_{cl}(+30$ V) or/and $H_{cl}(-30$ V), the magnetic states before and after electric-field cycling [states (2) and (4) in Fig. 4(a)] differ: the shape of the magnetic hysteresis loop is modified [see Fig. 5(a)] and the electric-field cycles become hysteretic [Fig. 5(b)]. Both the reversible and the nonreversible cases are now discussed in more detail.

B. Reversible magnetization reorientation

The electric-field-induced reversible variation of the sample magnetic state is rather easy to understand, following the discussion of Sec. III. Indeed, as H_p is greater than $H_{cl}(+30$ V) and $H_{cl}(-30$ V), the magnetic state is expected to remain homogeneous during the electric cycle. Moreover, as it can be seen in Fig. 5(a) for $H_p = 200$ Oe, the electric cycle produces an excursion of $M_\perp$ between the two reference magnetic hysteresis loops. This strongly suggests the magnetization direction to be continuously tilted by electric field, following the easy axis reorientation shown in Figs. 3(d)–3(f).

This electric-field-induced reversible $M_\perp$ variation was studied for different H orientations and magnitudes. As it was already described above, in Fig. 3(g), $M_\perp/M_s = \cos\theta$ is found to decrease when V_G is decreased from +30 to −30 V, thus reflecting a weakening of the out-of-plane magnetic anisotropy. Moreover, the predicted easy-axis reorientations, deduced from anisotropy-fields measurements, are quite similar to our observations, and present a quite good quantitative agreement. This can be checked also in Fig. 5(b), where the predicted variation of $M_\perp$ is reported along with the experimental data. The slightly larger mismatch observed in Fig. 3(g) close to $V_G = -30$ V most probably originates from the weakening of magnetic anisotropy, which makes the system more sensitive to anisotropy inhomogeneities, as discussed in Sec. III. The observed agreement confirms that the electric-field-controlled reversible variation of the system magnetic state is compatible with a continuous and coherent reorientation of the easy magnetization direction.

C. Nonreversible magnetization reversal

Let us now examine the electric-field-driven irreversible variations of the magnetization. The response of $M_\perp$ to a

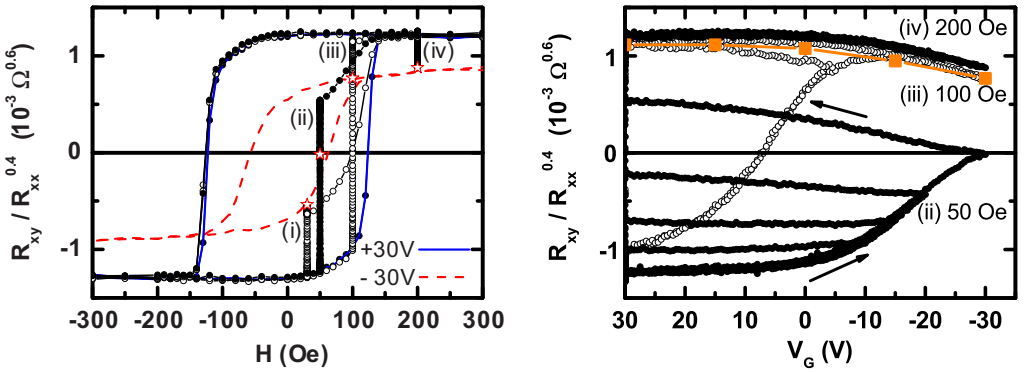

FIG. 5. (Color online) (a) Magnetic-field dependence of the Hall resistance at 15 K, with the magnetic field applied at $\theta_H = 50°$ from [001], in the (010) plane ($\varphi_H = 45°$). The solid- and dashed-line loops (reference loops) were measured under a constant gate voltage ($V_G = \pm 30$ V, respectively). For the other loops, the initial gate voltage was +30 V. After saturation under $H = -6$ kOe, the magnetic field was fixed at (i) $H_p = 30$, (ii) 50, (iii) 100, and (iv) 200 Oe, and the gate voltage was varied (≈ 1 V s^{-1}) from +30 to −30 V, where the point indicated by a star was reached. Then, V_G was increased back to +30 V, before the rest of the magnetic hysteresis loop was measured. (b) Gate-voltage dependence of the Hall resistance, measured for a larger selection of electric-field cycles under fixed magnetic fields. Large square symbols indicate the predictions of our free-energy-minimization model for $H = 200$ Oe, for comparison.

variation of V_G was studied for different H_p and $V_{G\min}$ values, as reported in Figs. 5(a) and 5(b). When $H_p < H_{cl}$, the evolution of the magnetic state can both result from the nucleation of magnetic domains and from the propagation of domain walls, and the interpretation of the results is thus more delicate.

As it can be observed in Fig. 5(b), a variation of V_G from +30 V to a negative $V_{G\min}$ [from (2) to (3) in Fig. 4(a)] results in an increase of $M_\perp$. A typical example is obtained for $H_p = 50$ Oe, which reveals the variation of $M_\perp$ to increase as $V_{G\min}$ is decreased between −10 and −30 V. The curves obtained for different $V_{G\min}$ values are superimposed, which reflects a reproducible change of the sample magnetic state. Moreover, a comparison between the results obtained for a same $V_{G\min} = -30$ V and for different values of H_p (30, 50, and 100 Oe), reveals the increase of $M_\perp$ to present a strong variation with the pause field. Namely, the $M_\perp$ values reached for $V_{G\min} = -30$ V for different pause fields are indicated by stars in Fig. 5(a). As it can be observed, those values are very close to the reference magnetic hysteresis loop recorded for $V_G = -30$ V [dashed line in Fig. 5(a)]. This feature suggests that the V_G decrease essentially results in a passage from one reference hysteresis loop to the other.

However, the evolution of $M_\perp$ recorded during a V_G increase [from (3) to (4) in Fig. 4(a)] is more surprising. As it can be observed in Fig. 5(b) for $H_p = 50$ Oe, $M_\perp$ is found to remain constant (for $V_{G\min} = -10$ and −15 V) or even to increase (for $V_{G\min} = -20$ and −30 V). This was observed both under out-of-plane and canted magnetic field. In order to analyze these results, it is important to separate the contribution of reversible magnetization reorientation within each domain, described in the previous section, from the contribution of an (irreversible) variation of the magnetic domain structure in the system. The open shape of magnetic hysteresis loops observed for instance in Fig. 4(b) indicates that at least two stable magnetic states coexist for $H = 0$, with only two well-defined values of the out-of-plane magnetization projection $\pm M_s \cos\theta$. Therefore, the resulting out-of-plane magnetization can be written as $M_\perp(V_G, H_p) = [M_s v_+ - M_s(1 - v_+)]\cos\theta$, where v_+ is the volume fraction of reversed domains. For $H_p = 200$ Oe, the magnetization is homogeneous ($v_+ = 1$), thus $M_\perp(V_G, 200\text{ Oe}) = M_s \cos\theta(V_G, 200\text{ Oe})$. In the 30–200 Oe H_p range, we can assume that $\cos\theta(V_G, H_p) \approx \cos\theta(V_G, 200\text{ Oe})$ since the variation of $\cos\theta$ with V_G is at least 2–3 times larger than with H_p [Fig. 5(a)]. This leads us to

$$v_+(V_G, H_p) \approx \frac{1}{2}\left[\frac{M_\perp(V_G, H_p)}{M_\perp(V_G, 200\text{ Oe})} + 1\right]. \qquad (2)$$

The evolution of v_+ with V_G is reported in Fig. 6(a), for $H_p =$ 50 and 100 Oe. As it can be seen, a decrease of V_G results in a systematic increase of v_+, therefore allowing the passage from one reference magnetic hysteresis loop to the other, as described above. However, for a V_G increase, v_+ may either remain almost constant or significantly increase, which cannot result from the same process.

Let us now discuss qualitatively these processes in the light of our understanding of electric-field effects on magnetic anisotropy. As it can be seen, for example, on the $V_G = -30$ V reference hysteresis loop in Fig. 5(a), the anisotropy reduction results in a magnetic softening of the system, classically driven by a reduction of domain-nucleation and domain-wall-propagation characteristic fields [30]. When decreasing V_G under a fixed H_p, the difference between the applied magnetic field and the nucleation and propagation fields is thus reduced. This should enhance nucleation of reversed domains, and/or expansion of reversed domains already present in the system by propagation of their domain walls, in agreement with our experimental observations.

In contrast, increasing V_G back to positive values should result in increasing back the nucleation and propagation fields, and therefore in freezing domain nucleation and domain-wall propagation. This does not explain *a priori* the further evolution of v_+ observed experimentally. However, a variation of the bilayer magnetic anisotropy also results in a change in

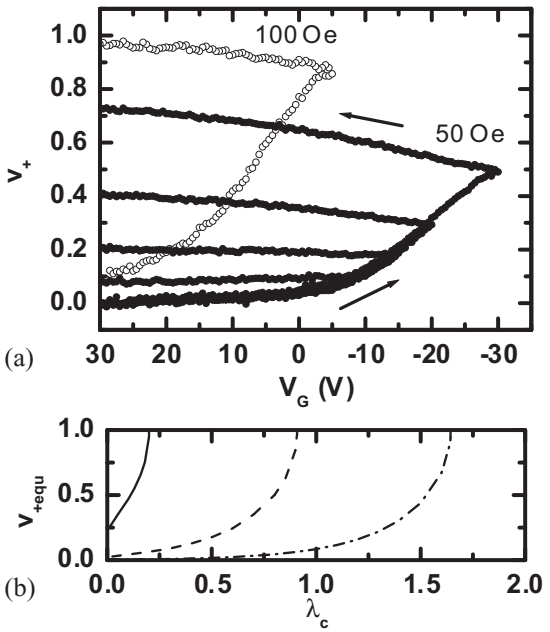

FIG. 6. (a) Gate-voltage dependence of the volume fraction of reversed domains v_+, measured at 15 K during electric-field cycles under a fixed magnetic field, applied at $\theta_H = 50^\circ$ from [001], in the (010) plane ($\varphi_H = 45^\circ$). The initial gate voltage was +30 V. After saturation under $H = -6$ kOe, the magnetic field was fixed at $H_p = 50$ and 100 Oe, respectively. The gate voltage was then decreased ($\approx 1\,\mathrm{V\,s^{-1}}$), and finally increased back to +30 V. (b) Predicted variation of the reduced magnetization $M_\perp/M_s = v_{+\mathrm{equ}}$, for different values of the reduced applied magnetic field $h = H/M_s$ (dashed-dotted line: $h = 0.003$; dashed line: $h = 0.03$; solid line: $h = 0.3$), as a function of the critical length $\lambda_c = \sigma/(\mu_0 M_s^2 e)$, where e is the ferromagnetic-film thickness, and σ is the domain-wall surface energy.

the domain-wall surface energy $\sigma \propto \sqrt{AK}$, where K is the anisotropy constant, and A is the exchange stiffness [31]. As the magnetic domain structure is driven by a balance between the stray-field energy, the pinning of domain walls, and the domain-wall surface energy, an anisotropy variation is thus expected to favor a reorganization of the domain structure. Qualitatively, considering only projections onto the out-of-plane direction, the expected sign of the resulting v_+ variation can be deduced from a simple model describing the evolution of the domain structure, at equilibrium and without pinning, in a magnetic film with perpendicular anisotropy submitted to an out-of-plane applied magnetic field [32]. Figure 6(b) shows the predicted variation of the reduced magnetization $M_\perp/M_s = v_{+\mathrm{equ}}$, for different values of the reduced applied magnetic field $h = H/M_s$, as a function of the critical length $\lambda_c = \sigma/(\mu_0 M_s^2 e)$, where e is the ferromagnetic-film thickness. As it can be observed, for a constant positive h value, increasing λ_c, i.e., increasing the anisotropy, results in an increase of $v_{+\mathrm{equ}}$. For our experiments, this means that v_+ can still evolve in some cases when V_G increases back to positive values, and that this evolution occurs following the polarity of the applied magnetic field. This is compatible with our experimental observation: under a positive magnetic field, an increase in V_G, thus in the anisotropy, results in an increase in v_+, rather than in a decrease. The reversed magnetic state ($M_\perp > 0$) is favored, as compared to the initial state ($M_\perp < 0$).

A practical consequence of nonreversible electric-field effects on v_+ is that an electric cycle can be used to partially or completely reverse the magnetization in the Hall bar, under a magnetic field lower than the bilayer coercive field. Examples of such electric-field-assisted switching are visible in Figs. 4(b) and 5(a), where an electric cycle between $V_G = +30$ and -30 V results in a nearly complete magnetization reversal. Such a complete electric-field-driven magnetization reversal is of particular interest, both conceptually and in the view of applications, as a simple approach to control the magnetic state of a system with an electric voltage.

V. CONCLUSION

In conclusion, we have studied electric-field-induced magnetization reorientation in a (Ga,Mn)As/(Ga,Mn)(As,P) bilayer with competing in-plane and out-of-plane anisotropies, embedded in a field-effect architecture. By applying an electric field, the relative carrier concentration in each layer, and thereby the magnetic anisotropy of the bilayer, could be controlled and the magnetization direction tilted. Both reversible and nonreversible magnetization changes were evidenced under a varying gate voltage as compared to the initial bilayer magnetic state, while staying relatively far from the Curie temperature, thus with low thermal fluctuations.

Within the reversible part of the magnetic hysteresis loop, the electric field produces a reorientation of the homogeneous magnetization of the sample. A variation of the electric field between $\pm 5.5\,\mathrm{MV\,cm^{-1}}$ allows us to tilt an initially perpendicular magnetization by an angle close to 60° in zero applied magnetic field. As this value is about five times larger than the reported magnetization tilt angle in a single layer [3], our study is a new step towards electric-field-induced irreversible magnetization reversal.

For the irreversible part of the magnetic hysteresis loop, the contribution of the electric field depends on the magnetic history of the sample. A gate-voltage cycling is found to essentially favor the magnetization reversal already started by the magnetic field. In particular, an almost complete magnetization switching driven by electric field, under a magnetic field smaller than the bilayer coercive field, was demonstrated. In addition to magnetization tilting, the reduction of the perpendicular anisotropy by an electric field is found to favor nucleation of magnetization reversal. Moreover, increasing back the perpendicular anisotropy also results in magnetization reversal. This observation is compatible with the prediction of models of self-organized domain structures for increasing domain-wall energy. In order to analyze in further detail the relative contributions of those different mechanisms to magnetization reversal, it would be particularly interesting to observe the evolution of the sample magnetic state by Kerr microscopy.

Eventually, these results are of particular interest in the search for ways of controlling the state of a magnetic system with an electric voltage, for example, to write or manipulate magnetic information. In this context, our approach and model

can be useful for designing and understanding improved structures for such purposes. More generally, electric-field effects on magnetic domain nucleation and domain-wall propagation currently motivate a growing interest in the community. Although qualitative conclusions are driven from this work, many questions still remain open, and deserve further investigation.

ACKNOWLEDGMENTS

J. Ferré is gratefully acknowledged for discussion and for a critical reading of the manuscript. This work was supported by the Agence Nationale de la Recherche (ANR MANGAS 2010-BLANC-0424). This work was also partly supported by the RENATECH network.

[1] D. Chiba, M. Yamanouchi, F. Matsukura, and H. Ohno, Science **301**, 943 (2003).
[2] M. Weisheit, S. Fähler, A. Marty, Y. Souche, C. Poinsignon, and D. Givord, Science **315**, 349 (2007).
[3] D. Chiba, M. Sawicki, Y. Nishitani, Y. Nakatani, F. Matsukura, and H. Ohno, Nature (London) **455**, 515 (2008).
[4] T. Maruyama, Y. Shiota, T. Nozaki, K. Ohta, N. Toda, M. Mizuguchi, A. A. Tulapurkar, T. Shinjo, M. Shiraishi, S. Mizukami, Y. Ando, and Y. Suzuki, Nat. Nanotechnol. **4**, 158 (2009).
[5] D. Chiba, S. Fukami, K. Shimamura, N. Ishiwata, K. Kobayashi, and T. Ono, Nat. Mater. **10**, 853 (2011).
[6] D. Chiba, Y. Nakatani, F. Matsukura, and H. Ohno, Appl. Phys. Lett. **96**, 192506 (2010).
[7] P. Balestrière, T. Devolder, J.-V. Kim, P. Lecoeur, J. Wunderlich, V. Novák, T. Jungwirth, and C. Chappert, Appl. Phys. Lett. **99**, 242505 (2011).
[8] Y. Shiota, T. Nozaki, F. Bonell, S. Murakami, T. Shinjo, and Y. Suzuki, Nat. Mater. **11**, 39 (2012).
[9] W.-G. Wang, M. Li, S. Hageman, and C. L. Chien, Nat. Mater. **11**, 64 (2012).
[10] D. Chiba, T. Ono, F. Matsukura, and H. Ohno, Appl. Phys. Lett. **103**, 142418 (2013).
[11] A. J. Schellekens, A. van den Brink, J. H. Franken, H. J. M. Swagten, and B. Koopmans, Nat. Commun. **3**, 847 (2012).
[12] D. Chiba, M. Kawaguchi, S. Fukami, S. Ishiwata, K. Shimamura, K. Kobayashi, and T. Ono, Nat. Commun. **3**, 888 (2012).
[13] E. Mikheev, I. Stolichnov, Z. Huang, A. W. Rushforth, J. A. Haigh, R. P. Campion, K. W. Edmonds, B. L. Gallagher, and N. Setter, Appl. Phys. Lett. **100**, 262906 (2012).
[14] I. Stolichnov, S. W. E. Riester, H. J. Trodahl, N. Setter, A. W. Rushforth, K. W. Edmonds, R. P. Campion, C. T. Foxon, B. L. Gallagher, and T. Jungwirth, Nat. Mater. **7**, 464 (2008).
[15] M. H. S. Owen, J. Wunderlich, V. Novák, K. Olejník, J. Zemen, K. Výborný, S. Ogawa, A. C. Irvine, A. J. Ferguson, H. Sirringhaus, and T. Jungwirth, New J. Phys. **11**, 023008 (2009).
[16] M. Sawicki, D. Chiba, A. Korbecka, Y. Nishitani, J. A. Majewski, F. Matsukura, T. Dietl, and H. Ohno, Nat. Phys. **6**, 22 (2010).
[17] T. Niazi, M. Cormier, D. Lucot, L. Largeau, V. Jeudy, J. Cibert, and A. Lemaître, Appl. Phys. Lett. **102**, 122403 (2013).
[18] A. Lemaître, A. Miard, L. Travers, O. Mauguin, L. Largeau, C. Gourdon, V. Jeudy, M. Tran, and J.-M. George, Appl. Phys. Lett. **93**, 021123 (2008).
[19] Y. Nishitani, D. Chiba, M. Endo, M. Sawicki, F. Matsukura, T. Dietl, and H. Ohno, Phys. Rev. B **81**, 045208 (2010).
[20] M. Cubukcu, H. J. von Bardeleben, K. Khazen, J. L. Cantin, O. Mauguin, L. Largeau, and A. Lemaître, Phys. Rev. B **81**, 041202 (2010).
[21] S. Kim, H. Lee, T. Yoo, S. Lee, S. Lee, X. Liu, and J. K. Furdyna, J. Appl. Phys. **107**, 103911 (2010).
[22] W. Limmer, J. Daeubler, L. Dreher, M. Glunk, W. Schoch, S. Schwaiger, and R. Sauer, Phys. Rev. B **77**, 205210 (2008).
[23] S. Onoda, N. Sugimoto, and N. Nagaosa, Phys. Rev. B **77**, 165103 (2008).
[24] M. Glunk, J. Daeubler, L. Dreher, S. Schwaiger, W. Schoch, R. Sauer, W. Limmer, A. Brandlmaier, S. T. B. Goennenwein, C. Bihler, and M. S. Brandt, Phys. Rev. B **79**, 195206 (2009).
[25] D. Chiba, A. Werpachowska, M. Endo, Y. Nishitani, F. Matsukura, T. Dietl, and H. Ohno, Phys. Rev. Lett. **104**, 106601 (2010).
[26] T. Jungwirth, Q. Niu, and A. H. MacDonald, Phys. Rev. Lett. **88**, 207208 (2002).
[27] R. Allenspach, J. Magn. Magn. Mater. **129**, 160 (1994).
[28] N. Bergeard, J.-P. Jamet, J. Ferré, A. Mougin, and J. Fassbender, J. Appl. Phys. **108**, 103915 (2010).
[29] X. Liu, W. L. Lim, L. V. Titova, M. Dobrowolska, J. K. Furdyna, M. Kutrowski, and T. Wojtowicz, J. Appl. Phys. **98**, 063904 (2005).
[30] J. Ferré, in *Spin Dynamics in Confined Magnetic Structures I*, Topics in Applied Physics Vol. 83, edited by B. Hillebrands and K. Ounadjela (Springer, Berlin, 2002), pp. 127–165.
[31] A. Hubert and R. Schäfer, *Magnetic Domains–The Analysis of Magnetic Microstructures* (Springer, Berlin, 1998).
[32] A. N. Bogdanov and D. A. Yablonskii, Fiz. Tverd. Tela (Leningrad) **22**, 680 (1980) [Sov. Phys. Solid State **22**, 399 (1980)].